EVALUATION OF STRESS IN BMI-CARBON FIBER LAMINATE TO DETERMINE THE ONSET OF MICROCRACKING

A Thesis

by

BRENT DURRELL PICKLE

Submitted to the Office of Graduate Studies of
Texas A&M University
in partial fulfillment of the requirements for the degree of

MASTER OF SCIENCE

December 2004

Major Subject: Mechanical Engineering

EVALUATION OF STRESS IN BMI-CARBON FIBER LAMINATE TO DETERMINE THE ONSET OF MICROCRACKING

A Thesis

by

BRENT DURRELL PICKLE

Submitted to Texas A&M University
in partial fulfillment of the requirements
for the degree of

MASTER OF SCIENCE

Approved as to style and content by:

Roger Morgan (Co-Chair of Committee)	Vikram Kinra (Member)
J. N. Reddy (Co-Chair of Committee)	Dennis O'Neal (Head of Department)

December 2004

Major Subject: Mechanical Engineering

ABSTRACT

Evaluation of Stress in BMI-Carbon Fiber Laminate to Determine

the Onset of Microcracking. (December 2004)

Brent Durrell Pickle, B.S., University of Oklahoma

Co-Chairs of Advisory Committee: Dr. R. Morgan
Dr. J. Reddy

In this work the conditions for which a $(0,90,90,0,0,90)_s$ BMI-carbon fiber laminate will initiate transverse microcracking are determined for the fabrication of a cryogenic fuel tank for use in a Reusable Launch Vehicle (RLV). This is accomplished using a quadratic interaction criterion failure analysis on the total stress state at possible launch conditions. There are three major sources of stress, that is, thermal residual stress, internal pressure stress, and applied load stress, that are evaluated at the launch stage to determine the total stress state. To assess the accuracy of the analysis the well known X-33 cryogenic fuel tank failure was analyzed as an example. The results of the X-33 example show that the analysis accurately portrays the failure of the X-33 and provides evidence that the analysis can be used to provide reliable conditions for the initiation of microcracking. The final result of this study is a range of launch conditions that can be used without the initiation of microcracking and a limiting range of conditions that cause complete microcracking throughout the laminate.

ACKNOWLEDGEMENTS

The author would like to thank the people who played an influential role in the development of this work. First, I thank Dr. R. Morgan for his academic supervision and leadership in serving as my primary research advisor and committee co-chair. Dr. J. Reddy also co-chaired the committee and provided excellent technical guidance. Their academic supervision made this work possible. Dr. V. Kinra is also due recognition for his time and interest in serving on this committee. In addition, I thank my family for their encouragement.

TABLE OF CONTENTS

LIST OF TABLES

LIST OF FIGURES

CHAPTER I

INTRODUCTION AND OVERVIEW

Reusable launch vehicles (RLV) are being designed as future space transportation systems. The propulsion system of the RLV uses cryogenic fuel stored in a structure that can be approximated by a cylinder with typical dimensions of 3 m. in radius and 10 m. in length [1]. This cylindrical fuel tank must be constructed of a lightweight material capable of withstanding the stresses incurred in the flight cycle of the RLV. The fuel tank will be exposed to a temperature range of 77 K to 420 K (about -196 ºC to 150 ºC), high accelerations, and an internal pressure during the flight cycle. A bismaleimide (BMI)-carbon fiber composite is being considered for this application due to its excellent thermal performance and ease of processing [2]. In considering this material for construction of the fuel tank it is essential to understand the stress that the laminated composite would be required to endure. The objective of this thesis is to evaluate and analyze the stress in the composite fuel tank.

The BMI-carbon fiber composite being considered for the fuel tank construction is a orthotropic 12 layer laminate approximately 1 in. thick with a lamination scheme of $(0,90,90,0,0,90)_s$. The critical failure mechanism for this laminate when used in this application is transverse microcracking, that is, microcracking that occurs transverse to the fiber direction in the lamina. A previous study was performed to characterize the development of microcracks in this laminate under mechanical stress and thermal

---

This thesis follows the style of *Journal of Composite Materials*.

cycling, simulating a typical flight cycle [2,3]. It was found that microcracks may form in the composite matrix when at the lowest temperatures of the cycle. This is due, in part, to the lower temperatures causing an increase in thermal residual stress as a result of thermal expansion mismatch between the fiber and the matrix [2,4,5]. This indicates that the most critical stage in the flight cycle will be when the tanks have just been filled and the RLV is taking off, that is, when the lowest temperatures are present and the acceleration is the greatest. It is at this stage in the flight cycle that the stress analysis will be performed to determine if microcracking will occur. There are 3 major sources of stress that contribute to the possible initiation of microcracks at this stage: thermal residual stress, internal pressure, and accelerated load.

As stated, thermal residual stresses appear as a result of the composite being below its stress free temperature, T_{SFT} [4,5]. During the curing process of the composite, its temperature is elevated to initiate and progress crosslinking. When the crosslinking stage of curing is complete the composite is assumed to be in a stress free state. The temperature in which this stage is completed is considered to be T_{SFT} [6]. For the purposes of calculating the thermal residual stresses, it has been shown that the T_{SFT} can be approximated by the glass transition temperature. The BMI-carbon fiber composite has a glass transition temperature of 511 K, therefore $T_{SFT} = 511$ K [7]. This is relatively high in comparison to the cryogenic temperature, 77 K, that will be seen by the composite and therefore the fuel tank will experience significant thermally induced stress.

In addition to the low mean temperature of the fuel tank, the wall of the fuel tank will have a through thickness temperature differential. The stage in the flight cycle being considered is just after the tanks have been filled. Looking at the worst instance in this stage the temperature of the inside of the wall will be the same as the cryogenic fuel, 77 K, while the outside of the tank wall will still be at ambient temperature, 300 K. This will produce a thermal bending stress that will also contribute to the stress seen in the composite.

The second source of stress is the internal pressure that will be required to store the cryogenic fuel. The pressure seen on the inside of the fuel tank will be approximately 290 kPa (42 psi) [1]. This will cause both a circumferential stress and a longitudinal stress in the fuel tank that will need to be evaluated.

The last major source of stress is the weight of the fuel load at take off. The maximum acceleration of the RLV in the direction of travel will be approximately of 1.5 g. It is also possible to experience acceleration in a direction lateral to the direction of flight of up to the 1 g. The fuel weight of approximately 210,000 lb and the accelerations imposed by the flight cycle will add to the stress in the fuel tank [1].

The procedure to evaluate the stress in the 12 layer BMI-carbon fiber laminate will be analytical. Laminated Plate Theory will be applied to the problem to solve the thermal residual stress. This method is commonly used to solve problems of this nature [5,6,8-10]. The stress due to internal pressure and accelerated loading will be evaluated using basic solid mechanics. These methods are well documented and accepted for such applications [11]. Once the stress state of the laminate is found, the stress will be

analyzed using the quadratic interaction criterion [12]. The findings will determine if flight cycle conditions will cause the onset of transverse microcracking in the laminate. Not only will the onset of transverse microcracking be determined, but a progressive failure analysis will show the extent of microcracking through the plies of the laminate. Also, as a specific example, the well documented X-33 RLV cryogenic fuel tank failure will be looked at and used as a test case for the analysis method. This failure is described in the following chapter.

The results of this study will provide valuable information that can be applied to any cryogenic fuel tank design. The focus of this thesis, however, will offer a unique and beneficial assessment of using a BMI-carbon fiber laminate in the design and fabrication of the RLV fuel tank.

CHAPTER II

X-33 FAILURE DESCRIPTION

There is a well documented case of a RLV fuel tank failure that will be analyzed in this thesis as an example and as a benchmark for calculation accuracy. The failure occurred during testing of the X-33, a prototype RLV developed by NASA and Lockheed Martin. The prototype combined several new and untested technologies, one of which was a composite liquid hydrogen fuel tank. An investigation team studied the failure of the fuel tank and their final report revealed the cause of the failure to be microcracking [1].

The wall of the X-33 fuel tank consisted of two layers of a carbon fiber-epoxy composite around a honeycombed Kevlar core, as shown in Figure 1.

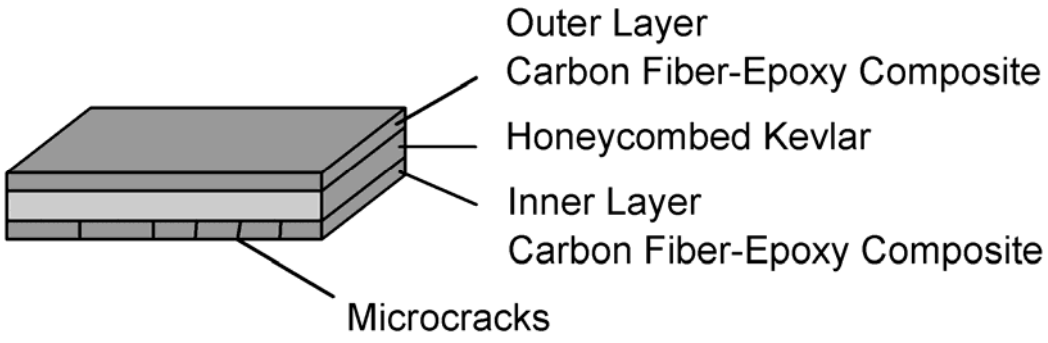

Figure 1. X-33 fuel tank wall section.

The major cause of the failure was extensive microcracking in the inside layer of the carbon fiber-epoxy composite. The microcracking occurred due to a combination of mechanical loading and thermal stress as the tank was filled with liquid hydrogen. Interconnecting of these microcracks allowed the hydrogen to infiltrate the honeycombed Kevlar. When the tank was subsequently emptied and the temperature began to rise, the microcracks closed trapping the hydrogen between the two layers of the carbon fiber-epoxy laminate. The hydrogen expanded as the temperature continued to increase, building up pressure in the honeycombed Kevlar until the outside layer of carbon fiber-epoxy composite ruptured. This agrees with the research by Ju and Morgan showing that microcracking can occur at cryogenic temperatures, and in this case microcracking can be considered the critical failure mechanism [2]. While the rupture was not directly caused by microcracking, it was the underlying reason that the failure occurred. Microcracking allowed permeation of the fuel through the laminate and, in the application of a pressurized fuel tank, permeability is critical property. Extensive microcracking such as this does also weaken the laminate and can lead to ultimate failure as well [13].

The X-33 program was halted soon after the failure of the fuel tank. The program ran 56 months with an overall cost of approximately $1.3 billion. Before the program was stopped, the redesign of the fuel tank was proposed to cost about $100 million [14]. This shows the significance of developing an analytical method to determining the onset and extent of microcracking, possibly preventing these costly failures.

From the description of the failure, insight can be gained into how the analysis should be performed. The most important thing shown in the X-33 failure was the critical mode of failure, that is, the extensive microcracking. Extensive microcracking can cause failure through permeability, as shown in the X-33 case, or through weakening of the laminate. In order to detect the onset and extent of microcracking in a laminate, an analysis of each ply is required. By looking at the laminate from the individual ply level, the onset of microcracking will be determined by the first ply to experience microcracking. The extent of microcracking will be shown by how many layers are microcracked.

In the following chapters the layer based analysis will be described and used to determine the state of microcracking in the BMI-carbon fiber composite. The specific case of the X-33 fuel tank failure will also be analyzed to determine if failure would have been predicted by the analysis methods described in this paper. In the analysis of the X-33, the inner laminate that experience microcracking will be looked at. The material used in this laminate is very similar to the BMI-carbon fiber laminate and therefore the material properties of the two will be considered the same. In essence the X-33 failure will be considered an experiment, testing the BMI-carbon fiber. The results of the failure will be used like those of an experiment to ascertain the accuracy of the analysis method presented in this thesis.

It is fortunate that such a detailed explanation of the X-33 failure was given. If the comparison of the actual failure and the analysis results validate the analysis method, then other conditions can be analyzed with a higher level of confidence. Looking at

other sets of conditions in addition to the X-33 failure should provide a good base of information to find the conditions that will initiate microcracking, and should offer support to recommendations for designing to deter microcracking.

CHAPTER III

STRESS ANALYSIS

As mentioned before, the analysis of this problem will be divided into three separate calculations: thermal residual stress, stress due to internal pressure, and stress caused by accelerated load. To analyze the fuel tank, a section of the tank wall will be approximated by a flat rectangular plate of the 12 layer $(0,90,90,0,0,90)_s$ BMI-carbon fiber laminated composite. The flat plate approximation can be used because the radius of the cylindrical tank is large and the slight curvature in a small section of the tank wall can be neglected. The plate will be oriented in a coordinate system as shown below in Figure 2.

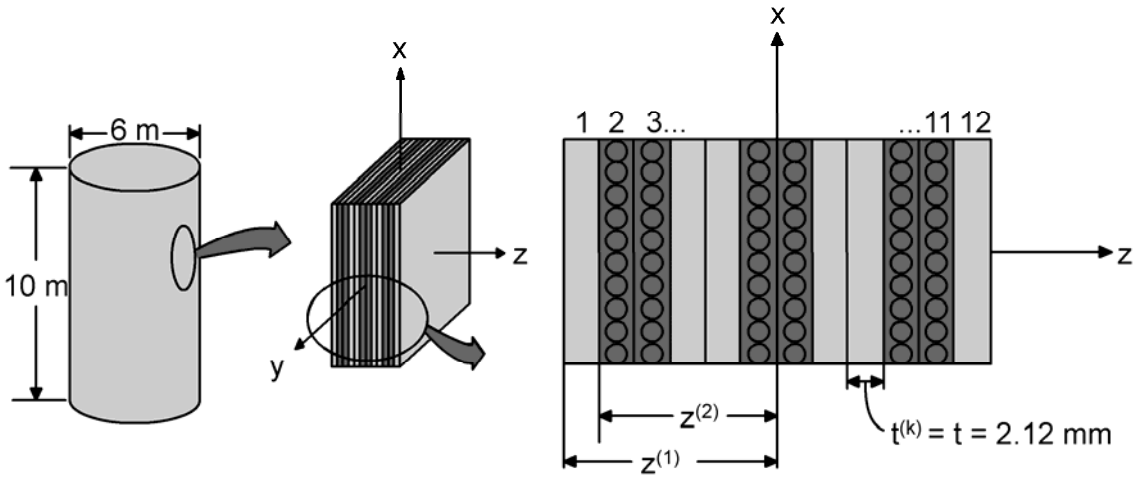

Figure 2. Detailed views of fuel tank with coordinate system and lamina numbering.

As shown, the x-y plane is the midplane of the laminate and the positive z direction is towards the outside of the tank. This will be the global coordinate system used for the stress analysis.

The following sections will describe the methods used to calculate the stress for each of the stress sources. A description of the quadratic interaction failure criterion is also given. Using this information, the stress state of each ply of the laminate will be evaluated to determine whether or not microcracking will occur.

THERMAL RESIDUAL STRESS

Laminated Composite Plate Theory (LCPT) will be used to obtain the stresses induced by the fuel tank being exposed to a cryogenic temperature. The derivation of this theory is detailed by Reddy [9]. LCPT offers a way to calculate thermal residual stresses, which is of interest in this study. The thermal stresses are given as force and moment resultants, $\{N^T\}$ and $\{M^T\}$ respectively. These quantities are thickness-averaged lamina forces and moments measured per unit width of the plate. Therefore, a force resultant has units [N/m] and a moment resultant has units [N-m/m]. They are defined for each layer of the laminate as

$$\left\{N^T\right\}^{(k)} = \int_{z_k}^{z_{k+1}} \left[Q\right]^{(k)} \left\{\alpha\right\}^{(k)} \Delta T \, dz \tag{3.1}$$

and

$$\left\{M^T\right\}^{(k)} = \int_{z_k}^{z_{k+1}} \left[Q\right]^{(k)} \left\{\alpha\right\}^{(k)} \Delta T \, z \, dz \tag{3.2}$$

where the superscript (k) denotes for which lamina the resultants are being calculated, $[Q]^{(k)}$ is the lamina stiffness matrix, $\{\alpha\}^{(k)}$ is the lamina thermal expansion coefficient matrix, ΔT is the temperature difference between a reference temperature and the current temperature, and z is the thickness coordinate [10]. In the present case the temperature varies linearly through the thickness coordinate of the plate and as a result the temperature difference should be written

$$\Delta T = T_0 + zT_1 \tag{3.3}$$

Here T_0 is the difference between the average temperature of the plate and the reference temperature and T_1 is the change in temperature per unit thickness of the plate.

The symmetry of the lamination scheme, lamina thicknesses, and lamina properties about the midplane of the laminate can be used to simplify the calculation. These symmetries eliminate the coupling between bending and extension and simplify the governing equations [10]. The symmetry reduced thermal resultants are given by Reddy as

$$\begin{Bmatrix} N_x^T \\ N_y^T \end{Bmatrix}^{(k)} = \int_{z_k}^{z_{k+1}} \begin{bmatrix} Q_{xx} & Q_{xy} \\ Q_{xy} & Q_{yy} \end{bmatrix}^{(k)} \begin{Bmatrix} \alpha_x \\ \alpha_y \end{Bmatrix}^{(k)} T_0 \, dz \tag{3.4}$$

and

$$\begin{Bmatrix} M_x^T \\ M_y^T \end{Bmatrix}^{(k)} = \int_{z_k}^{z_{k+1}} \begin{bmatrix} Q_{xx} & Q_{xy} \\ Q_{xy} & Q_{yy} \end{bmatrix}^{(k)} \begin{Bmatrix} \alpha_x \\ \alpha_y \end{Bmatrix}^{(k)} T_1 \, z^2 \, dz \tag{3.5}$$

where α_x and α_y are the thermal expansion coefficients in the x and y directions, and

$$Q_{xx}^{(k)} = \frac{E_x^{(k)}}{1 - \nu_{xy}^{(k)} \nu_{yx}^{(k)}} \tag{3.6}$$

$$Q_{xy}^{(k)} = \frac{\nu_{xy}^{(k)} E_y^{(k)}}{1 - \nu_{xy}^{(k)} \nu_{yx}^{(k)}} \tag{3.7}$$

$$Q_{yy}^{(k)} = \frac{E_y^{(k)}}{1 - \nu_{xy}^{(k)} \nu_{yx}^{(k)}} \tag{3.8}$$

Here $E_x^{(k)}$ and $E_y^{(k)}$ are the lamina longitudinal modulus and transverse modulus, respectively, and $\nu_{xy}^{(k)}$ and $\nu_{yx}^{(k)}$ are longitudinal and transverse Poisson's ratios.

Once the thermal force and moment resultants are obtained, they need to be converted to a stress to be useful for analysis. As previously stated the force and moment resultants are just the thickness-averaged lamina forces and moments per unit width of the plate. Using the definition of the force resultant, the thermal axial stress in the k^{th} lamina, $\{\sigma^N\}^{(k)}$, is obtained simply be dividing the force resultant by the thickness of the lamina, t.

$$\left\{\sigma^N\right\}^{(k)} = \begin{Bmatrix} \sigma_x^N \\ \sigma_y^N \end{Bmatrix}^{(k)} = \frac{1}{t} \begin{Bmatrix} N_x^T \\ N_y^T \end{Bmatrix}^{(k)} \tag{3.9}$$

The moment resultant for each ply is the moment per unit width caused by that ply on the laminate. Using basic mechanics the moment can be given as the product of a force in the ply and a moment arm, $D^{(k)}$. The moment arm is taken as the distance from the neutral axis of the plate to the center of the lamina. This is displayed graphically in Figure 3. Since the moment arm is a known value, the force in the lamina can be obtained by dividing the moment resultant by the moment arm. The resulting force will be per unit width of the plate, just as the moment resultant was per unit width.

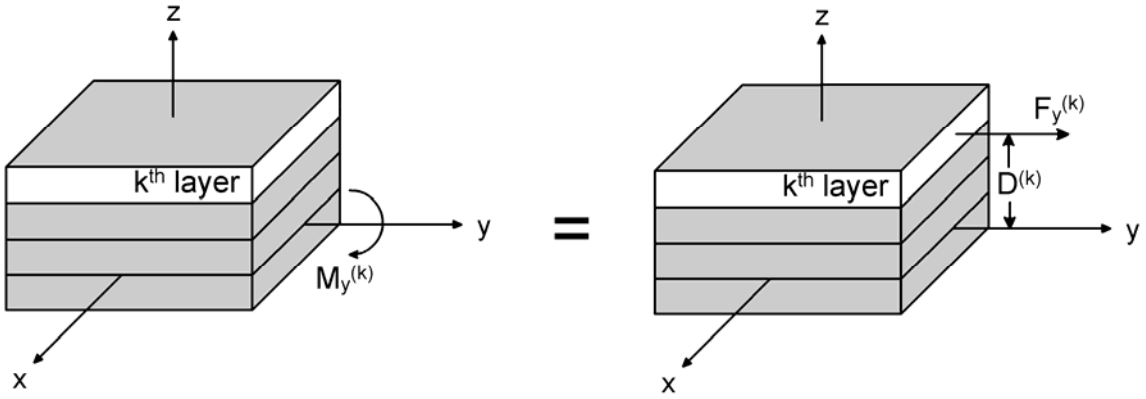

Figure 3. Separation of moment into force and moment arm.

Now the thermal bending stress in the k^{th} lamina, $\{\sigma^M\}^{(k)}$, can be calculated by dividing the force per unit width by the lamina thickness,

$$\left\{\sigma^M\right\}^{(k)} = \begin{Bmatrix} \sigma_x^M \\ \sigma_y^M \end{Bmatrix}^{(k)} = \frac{1}{(t)(D^{(k)})} \begin{Bmatrix} M_x^T \\ M_y^T \end{Bmatrix}^{(k)} \tag{3.10}$$

where $D^{(k)}$ is the moment arm

$$D^{(k)} = z^{(k)} + \frac{t}{2} \tag{3.11}$$

Using equations (3.9) and (3.10) the total thermal stress in the k^{th} lamina, $\{\sigma^T\}^{(k)}$, is given by

$$\left\{\sigma^T\right\}^{(k)} = \begin{Bmatrix} \sigma_x^T \\ \sigma_y^T \end{Bmatrix}^{(k)} = \frac{1}{t} \begin{Bmatrix} N_x^T \\ N_y^T \end{Bmatrix}^{(k)} + \frac{1}{(t)(D^{(k)})} \begin{Bmatrix} M_x^T \\ M_y^T \end{Bmatrix} \tag{3.12}$$

To summarize equations (3.4) and (3.5) are employed to find the force and moment resultants for each ply of the laminate. These values are then used with equation (3.12) to find the total thermal stress in each ply.

INTERNAL PRESSURE STRESS

The internal pressure required to store the cryogenic fuel in the tank also causes stress in the wall of the fuel tank. There are two stresses that result from an internal pressure, stress in the longitudinal direction and the circumferential direction, as shown in Figure 4 below.

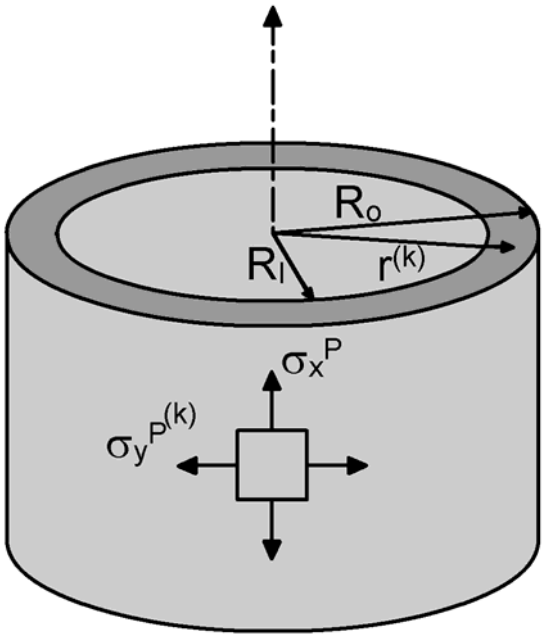

Figure 4. Stress due to internal pressure.

The longitudinal stress, corresponding to the x coordinate, is defined as

$$\sigma_x^P = \frac{P}{\left(\frac{R_O}{R_I}\right)^2 - 1} \tag{3.13}$$

and the circumferential stress, the y coordinate stress, is

$$\sigma_y^{p(k)} = \frac{P\left(1 + \left(\frac{R_O}{r^{(k)}}\right)^2\right)}{\left(\left(\frac{R_O}{R_I}\right)^2 - 1\right)} \tag{3.14}$$

where P is the internal pressure, R_O is the outside radius of the fuel tank, and R_I is the inside radius of the fuel tank [12]. The longitudinal stress is the same through all the layers of the laminate. The circumferential stress, however, varies slightly through the thickness of the laminate. In equation (3.14), $r^{(k)}$ appears as the radius to the point in which the stress is being calculated. In this case the points at which the circumferential stress will be calculated are the centers of the lamina in the z direction, therefore

$$r^{(k)} = z^{(k)} + \frac{t}{2} \tag{3.15}$$

APPLIED LOAD STRESS

The maximum applied load will occur at take off. This is when the fuel tank is completely full and the acceleration is the greatest. During take off the fuel tank will experience acceleration in both the x and y directions, a_x and a_y. The force of the load at these accelerations is simply

$$\begin{Bmatrix} F_x \\ F_y \end{Bmatrix} = m_f \begin{Bmatrix} a_x \\ a_y \end{Bmatrix} \tag{3.16}$$

where m_f is the mass of the fuel. The stress in each direction is found by merely divide the forces in equation (3.17) by the cross-sectional area of the cylinder in the x and y directions, A_x and A_y respectively. The result is

$$\begin{Bmatrix} \sigma_x^L \\ \sigma_y^L \end{Bmatrix} = \begin{Bmatrix} \dfrac{F_x}{A_x} \\ \dfrac{F_y}{A_y} \end{Bmatrix} \tag{3.17}$$

where $\{\sigma^L{}_x\}$ is the stress due to the loading in the x direction and $\{\sigma^L{}_y\}$ is the stress due to the loading in the y direction.

The lamination scheme for the laminate shows, however, that there will be six layers oriented parallel to the global x axis and six layers at 90º from the x axis. Since the elastic moduli for the layers are direction dependent, the two differently oriented groups will have different moduli of elasticity. This will cause the loading stresses to be divided unequally among the two groups. To find the distribution of stress in the groups basic mechanics is applied.

The strain in each group, ε^0 for the group parallel to the x axis and ε^{90} for the group at 90º to the x axis, is assumed to be equal. Strain, in terms of stress, σ, and the modulus of elasticity, E, is written

$$\varepsilon = \frac{\sigma}{E} \tag{3.18}$$

Since the strains of the two groups are assumed equal

$$\frac{\sigma^0}{E^0} = \frac{\sigma^{90}}{E^{90}} \tag{3.19}$$

where the superscripts denote the group associated with the stress and elastic moduli. Using equation (3.19) and the fact that the sum of stresses σ^0 and σ^{90} give the total stress in the laminate, σ^T, the distribution of the total stress in the two groups of differently oriented plies can be obtained. The stress in the parallel group is

$$\sigma^0 = \frac{E^0 \sigma^T}{\left(E^0 + E^{90}\right)} \tag{3.20}$$

Similarly the stress in the perpendicular group is

$$\sigma^{90} = \frac{E^{90} \sigma^T}{\left(E^0 + E^{90}\right)} \tag{3.21}$$

Putting these equations in terms of the current problem's coordinate system, the two stresses in the x and y directions are written from equations (3.20) and (3.21) as

$$\sigma_x^{0,90} = \frac{E^{0,90} \sigma_x^L}{(E^0 + E^{90})} \tag{3.22}$$

and

$$\sigma_y^{0,90} = \frac{E^{0,90} \sigma_y^L}{(E^0 + E^{90})} \tag{3.23}$$

where σ_x^L and σ_y^L are the stresses defined in Eq. (3.17).

QUADRATIC INTERACTION CRITERION

The analysis of the stresses defined in the three sections above is performed using the quadratic interaction criterion. A detailed description of this method is given

in the ASME pressure vessel code [12]. It appears to be similar to the Tsai-Wu failure criteria [10]. This criterion is used on each of the ply in the laminate to determine failure at a lamina level. In this criterion lamina failure includes failure in the transverse direction, that is, microcracking [13]. It will be shown that the transverse failure will be dominant as compared to failure in the fiber direction of the lamina. Therefore, when a lamina is said to have failed by this criterion, at least in the conditions of this problem, it means the lamina has experienced microcracking in the transverse direction. The quadratic interaction criterion is

$$R^2\left(F_{xx}\sigma_x^2 + 2F_{xy}\sigma_x\sigma_y + F_{yy}\sigma_y^2\right) + R\left(F_x\sigma_x + F_y\sigma_y\right) - 1 = 0 \tag{3.24}$$

where

$$F_{xx} = \frac{1}{X\,X_c} \tag{3.25}$$

$$F_{yy} = \frac{1}{Y\,Y_c} \tag{3.26}$$

$$F_x = \frac{1}{X} - \frac{1}{X_c} \tag{3.27}$$

$$F_y = \frac{1}{Y} - \frac{1}{Y_c} \tag{3.28}$$

and

$$F_{xy} = -\frac{1}{2}\sqrt{F_{xx}F_{yy}} \tag{3.29}$$

In the above equations X is the tensile strength in the fiber direction, X_c is the compressive strength in the fiber direction, Y is the tensile strength transverse to the

fibers, Y_c is the compressive strength transverse to the fibers, σ_x is the stress in the fiber direction, and σ_y is the stress transverse to the fibers. These properties and stresses are all properties and stresses of the individual lamina. R is the only unknown in the equation, and solving for R gives

$$R = \frac{-H \pm \sqrt{H^2 + 4G}}{2G} \tag{3.30}$$

where

$$G = F_{xx}\sigma_x^2 + 2F_{xy}\sigma_x\sigma_y + F_{yy}\sigma_y^2 \tag{3.31}$$

and

$$H = F_x\sigma_x + F_y\sigma_y \tag{3.32}$$

The value of R is taken as the positive of the two values obtained from Eq. (3.30). The quadratic interaction criterion states that if the applied stress components lead to $R < 1$, then the lamina will fail. If the result is $R > 1$, the lamina will not fail [12].

By looking at each lamina with this criterion a number of facts can be ascertained. The most important fact to be seen is whether or not the conditions imposed on the fuel tank will cause microcracking in any of the layers at all. If microcracking does exist, the extent of microcracking in the laminate can be found using a progressive failure analysis. This is done because as a layer fails the stresses in the other layers is increased. In order to take this increase of stress into account in the remaining unmicrocracked lamina the sources of the stress will be considered. The thermal stress in a lamina originates from the material within that lamina and therefore will not be increased by the failure of another lamina. The internal pressure and loading stresses,

however, are externally applied and the failure of one lamina will increase the remaining lamina stresses. The pressure stress will increase in proportion to the ratio of the total number of lamina to the total number of lamina that have not failed. The result of this can be expressed as

$$\sigma'_P = \frac{12}{N}(\sigma_P) \tag{3.33}$$

where σ_P' is the new pressure stress in the lamina, σ_p is the original pressure stress in the lamina, and N is the number of layers that remain not failed. This is in essence decreasing the area over which the original pressure force is applied. A similar expression can be written for the loading stress

$$\sigma'_L = \frac{12}{N}(\sigma_L) \tag{3.34}$$

where σ_L' is the new loading stress in the lamina, σ_L is the original loading stress in the lamina.

In the four previous sections, the necessary equations to evaluate the stress in each ply of the laminate and analyze the stresses were given. The results of these calculations will be presented and reviewed in the following chapter. The X-33 failure will also be analyzed and the results of the analysis will be compared to the actual outcome of the X-33 fuel tank. The results of the specific case will aid in validating the methods described in this chapter.

CHAPTER IV

RESULTS AND DISCUSSION

In this chapter the results of the previously described stress evaluation will be given. First, results will be given for the conditions that lead to the failure of the X-33. These results will then be compared to the actual outcome of the failure. After reviewing the X-33 failure, other sets of conditions will be considered in order to further assess the application of the BMI-carbon fiber laminate to the cryogenic fuel tank.

The material properties used in the stress evaluation are listed in Table 1 [2,7,15,16]. These are lamina properties where the subscript x denotes the property is in the fiber direction and the subscript y signifies the transverse direction.

Table 1. BMI-carbon fiber lamina material properties at 144 K.

Properties for Stress Calculation			Properties for Failure Criterion		
E_x	151.00	[GPa]	X	3.45	[GPa]
E_y	11.00	[GPa]	X_c	1.72	[GPa]
α_x	-0.43	[μm/m-K]	Y	93.80	[MPa]
α_y	18.10	[μm/m-K]	Y_c	197.00	[MPa]
ν_{xy}	0.34				
ν_{yx}	0.03				
t	2.12	[mm]			

Table 1 gives the material properties for the lamina at a temperature of 144 K. This temperature is used because it is approximately the average temperature in the wall of the fuel tank.

The conditions of the X-33 fuel tank that lead to failure are listed in Table 2 [1]. During the test when the tank failed there was no acceleration other than gravitational acceleration, and this is reflected in the calculations for the X-33 analysis. However, in the conditions used for further assessment of the laminate accelerations will be applied to as they occur at takeoff, that is, with upward and lateral accelerations of 1.5 g and 1 g.

Table 2. Conditions of X-33 fuel tank that caused failure.

Condition		
Fuel Temperature	77	[K]
Fuel Mass	95,250	[kg]
Internal Pressure	290	[kPa]
Acceleration, a_x	1	[g]
Lateral Acceleration, a_y	0	[g]

X-33 FAILURE ANALYSIS

Using the properties and conditions described in Table 1 and Table 2, the thermal stresses can be calculated for the inner laminate of the X-33 fuel tank. The thermal stresses are shown given Table 3 and Table 4. In the tables the thermal stresses are given in reference to the lamina fiber and transverse direction. A demonstration thermal stress calculation is given in Appendix A.

Table 3. X-33 lamina thermal stresses in lamina coordinates.

	Thermal Axial Stress [MPa]		Thermal Bending Stress [MPa]	
Layer	Fiber Direction	Transverse	Fiber Direction	Transverse
1	0.899	64.230	0.286	20.410
2	0.899	64.230	0.234	16.720
3	0.899	64.230	0.183	13.040
4	0.899	64.230	0.131	9.376
5	0.899	64.230	0.081	5.757
6	0.899	64.230	0.035	2.467
7	0.899	64.230	-0.035	-2.467
8	0.899	64.230	-0.081	-5.757
9	0.899	64.230	-0.131	-9.376
10	0.899	64.230	-0.183	-13.040
11	0.899	64.230	-0.234	-16.720
12	0.899	64.230	-0.286	-20.410

Table 4. X-33 lamina total thermal stress.

	Total Thermal Stress [MPa]	
Layer	Fiber Direction	Transverse
1	1.185	84.640
2	1.133	80.950
3	1.082	77.270
4	1.030	73.606
5	0.980	69.987
6	0.934	66.697
7	0.865	61.763
8	0.818	58.473
9	0.768	54.854
10	0.717	51.190
11	0.665	47.510
12	0.613	43.820

From the above tables, it can be seen that the thermal axial stresses in the fiber direction of the lamina are all equal. The thermal axial stresses in the transverse direction are all equal as well. This is expected due to the axial stress being calculated using the average temperature through the thickness of the wall, which will be the same for each ply. It is interesting that the stress in the transverse direction is much greater than the stress in the fiber direction. This is a consequence of the thermal expansion coefficient being much greater for the matrix than the fiber. The thermal bending stresses increase in magnitude with the increase in distance the ply is from the center of the wall. However, the plies on the inside of the fuel tank, layers 1 to 6, have a positive bending thermal stress and outer layers, 6 to 12, have a negative bending thermal stress. This means that the bending thermal stress decreases the total thermal stress on the outside of the wall while it increases the total thermal stress on the inside of the wall. This is intuitively correct because the temperature in the wall is lower on the inside of wall and thermal residual stress increases as the temperature of the lamina decreases. The largest total thermal stress occurs on the inside lamina of the fuel tank wall. The thermal stress in that lamina in the transverse direction is 84.64 MPa. This is important because the thermal stress alone is over 90% of the transverse strength, which is given in Table 1 as 93.80 MPa. It should also be noted that both the thermal axial and bending stress are symmetric about the midplane of the laminate as expected.

The next calculation to be made is the stress due to the internal pressure. A sample calculation is shown in Appendix B and the results are given in Table 5, below. The stress due to pressure in the longitudinal direction of the fuel tank, or the

global x direction, is constant throughout the laminate, while the circumferential stress, the global y direction, varies slightly through the thickness. The stresses in Table 5 are given in reference to the lamina fiber direction. It can be seen that the longitudinal stress is approximately half of the circumferential stress, which is consistent with the basic mechanics of thin-wall pressure vessels [11]. The maximum circumferential stress occurs in the inside lamina of the fuel tank wall in the transverse direction and is about 36% of the transverse strength. The constant longitudinal strength is about 18% of the transverse lamina strength.

Table 5. X-33 lamina stress due to internal pressure.

	Pressure Stress [MPa]	
Layer	Fiber Direction	Transverse
1	16.88	34.05
2	34.02	16.88
3	34.00	16.88
4	16.88	33.97
5	16.88	33.95
6	33.92	16.88
7	33.90	16.88
8	16.88	33.88
9	16.88	33.85
10	33.83	16.88
11	33.80	16.88
12	16.88	33.78

The stresses due to the applied load, the fuel stored in the tank, are evaluated next. An example calculation is documented in Appendix C. Given below in Table 6, the loading stresses are the smallest contributor to the overall stress in each lamina. As stated, the acceleration in the global y direction was 0 during the testing of the X-33 and the global x acceleration was simply gravitational acceleration. It should be noticed that the stresses in the transverse direction of the lamina are almost nonexistent. This is expected due to the fact that the modulus of each lamina in the fiber direction is much larger that the modulus in the transverse direction. This causes the loading to be distributed disproportionately to the lamina whose fiber direction is parallel to the global x coordinate. Again the loading stresses are very small, and the maximum transverse loading stress is about 0.1% of the transverse strength.

Table 6. X-33 lamina stress due to accelerated load.

	Load Stress [MPa]	
Layer	Fiber Direction	Transverse
1	1.81	0.00
2	0.00	0.13
3	0.00	0.13
4	1.81	0.00
5	1.81	0.00
6	0.00	0.13
7	0.00	0.13
8	1.81	0.00
9	1.81	0.00
10	0.00	0.13
11	0.00	0.13
12	1.81	0.00

To see the total stress state of each lamina in the X-33 fuel tank, the total stress is found by combining the above calculations. The result is given in Table 7, below.

Table 7. X-33 total stress in lamina.

	Total Stress [MPa]	
Layer	Fiber Direction	Transverse
1	19.88	118.69
2	35.15	97.96
3	35.08	94.28
4	19.72	107.58
5	19.67	103.94
6	34.85	83.71
7	34.76	78.77
8	19.51	92.35
9	19.46	88.70
10	34.55	68.20
11	34.46	64.52
12	19.30	77.60

The table of total stress shows that the maximum stress in each of the lamina occurs in the transverse direction. Since the transverse direction is also the direction of lowest strength for the lamina, this confirms that the critical failure mechanism of the lamina will be transverse microcracking. Moreover, the maximum transverse stress that occurs is 126% of the lamina transverse strength. The more in depth quadratic interaction failure analysis will be performed on all these lamina, however, from the fact that some

of the transverse stresses exceed the transverse strength at least some microcracking can be expected. A graphical view of the total stresses is shown in Figure 5.

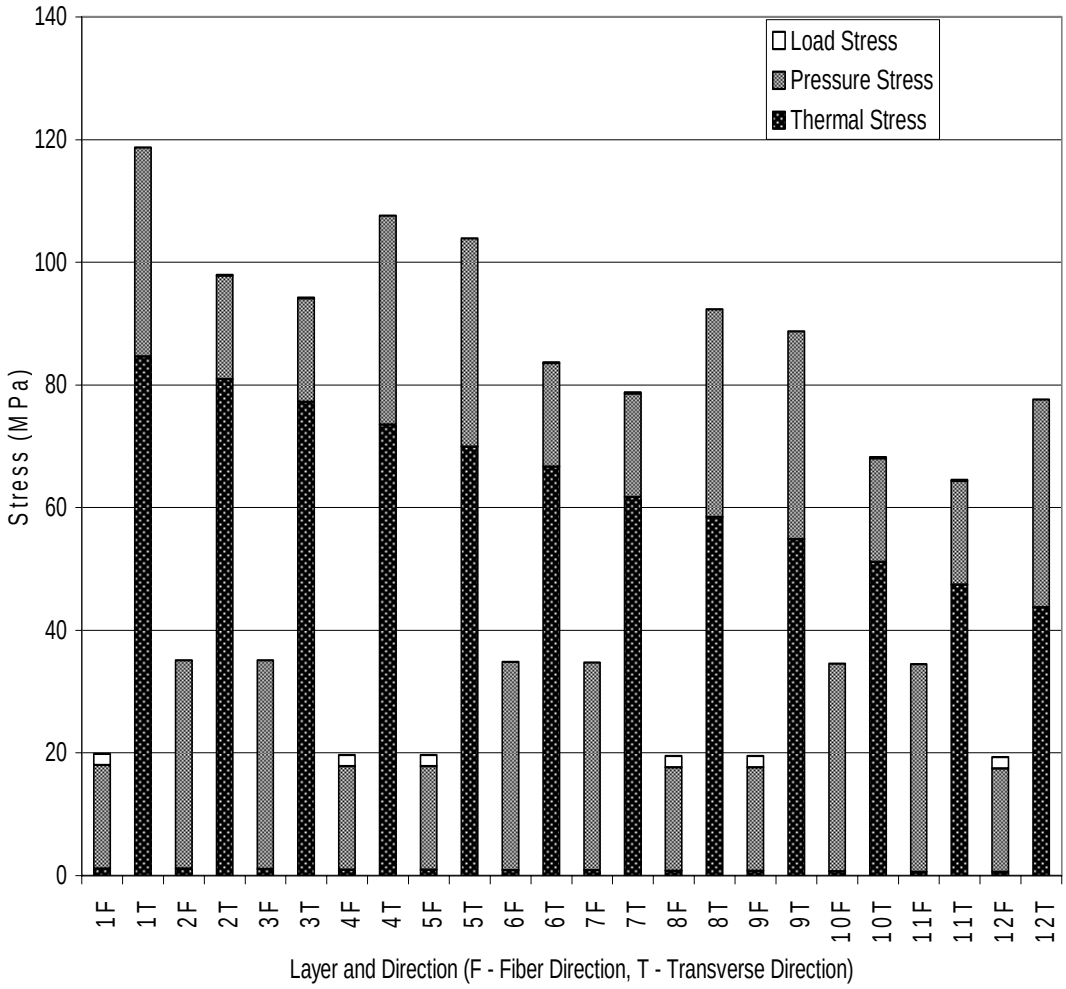

Figure 5. Total stress in the lamina of the X-33, in the fiber and transverse directions.

The above bar graph displays the total stress in each of the 12 lamina in both the fiber and transverse directions. The x-axis of the plot is marked with the lamina number and a letter, where F indicates that the stress is in the fiber direction and T indicates that the stress is in the transverse direction. The stress bars for each lamina are broken into three sections, as labeled on the graph. This graph illustrates many important details of the analysis. One point that can be observed is that the transverse stress does not decrease successively with each layer of the laminate moving from the inside of the wall to the outside. There is however a pattern to the general decrease in transverse stress from the inside to the outside of the wall. The pattern has to do with if the transverse direction of the lamina corresponds to the circumferential pressure stress. This alignment happens on the layers of the laminate that have their fiber direction parallel to the global x-axis. This makes the order of highest to lowest transverse stress nonconsecutive, when it may have been expected to be consecutive. This also indicates the sequence of layer failures will not be consecutive, but in the order of highest transverse stress to lowest. However, looking at the thermal stress alone, the darkest part of the stress bar, the transverse stress does decrease sequentially from the inner layer to the outer layer. The stress in the fiber direction is relatively small, and since the fiber direction strength is very large, any failure of the lamina in the fiber direction is unlikely.

Now that the stresses have been found, the quadratic interactive failure criterion can be applied, along with a progressive failure analysis. This was done and the results are shown in Table 8. The failure criterion is given in the R value, if $R < 1$ then failure occurs, while if $R > 1$ failure will not occur. Looking at the column representing the

analysis with no failed layers, the R value is less than one in four layers, thus four layers have failed. The layers that have failed are, in order of failure, 1, 4, 5, and 2. When this is taken into account through the progressive analysis the R values given in the column labeled four failed layers apply. Here the R values for an additional three layers have dropped below one. The three layers that failed are 3, 8, and 9. Taking these additional failures into account the next column of seven failed layers applies, which leads to using the column of ten failed layers. In this column none of the R values are above one which means that the laminate has experienced microcracking throughout the entire thickness of the wall. Therefore the final result of the X-33 fuel tank analysis is that the fuel tank wall will have extensive microcracking through wall of the tank, just as occurred in the actual test.

Table 8. X-33 progressive failure analysis.

	R Values Number of Failed Layers			
Layer	0	4	7	10
1	0.80	0.70	0.57	0.33
2	0.98	0.90	0.79	0.54
3	1.01	0.93	0.82	0.55
4	0.88	0.76	0.61	0.34
5	0.91	0.79	0.63	0.35
6	1.15	1.04	0.90	0.58
7	1.22	1.11	0.95	0.60
8	1.03	0.87	0.68	0.37
9	1.07	0.90	0.70	0.37
10	1.41	1.26	1.06	0.65
11	1.50	1.33	1.11	0.66
12	1.23	1.01	0.76	0.39

A graphical representation of Table 8 is given below in Figure 6. The graph shows the R value as a function of the number of layers that are not failed. The right side of the graph represents the analysis done with no failed layers, or as labeled on the

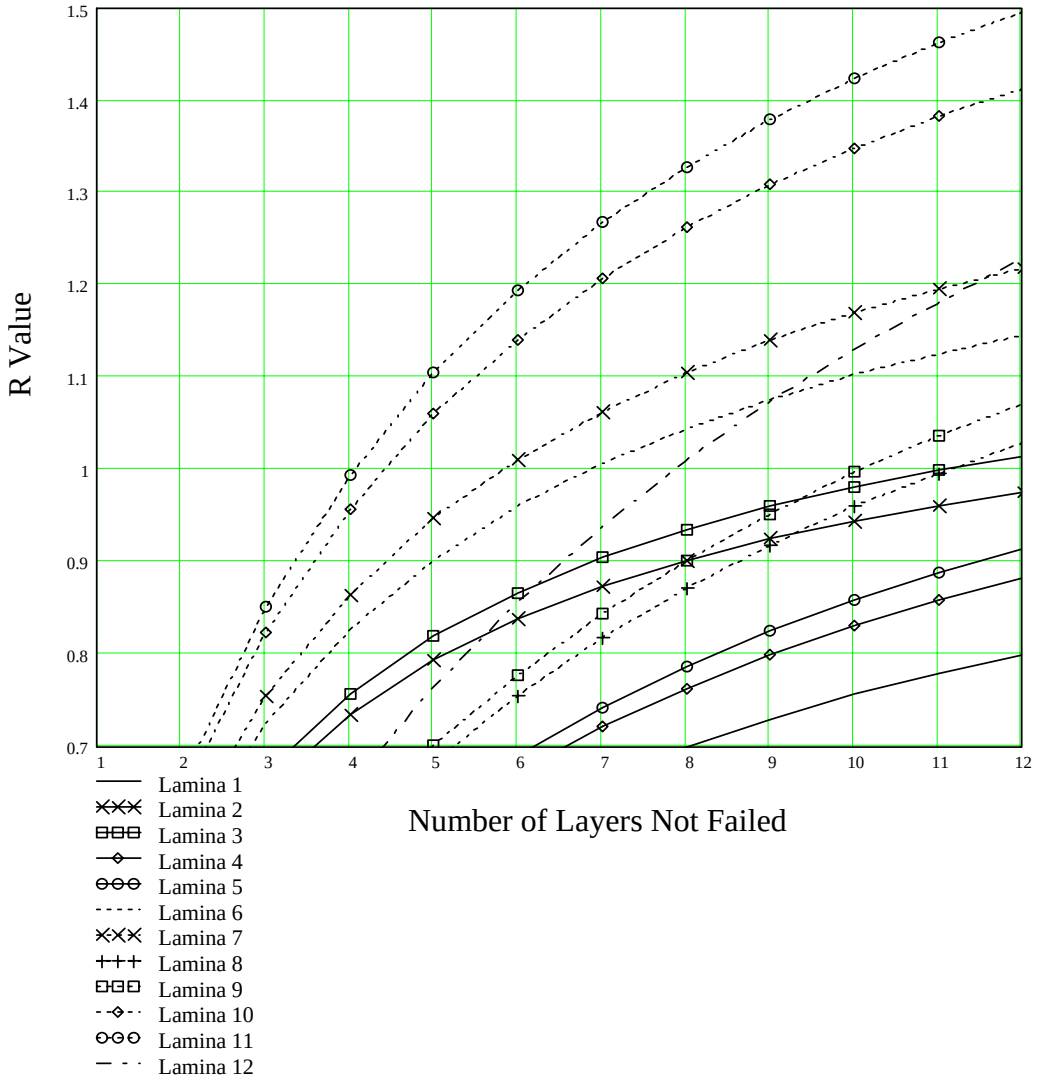

Figure 6. X-33 lamina R value as a function of layers not failed.

graph, with 12 layers not failed. Moving left on the graph the R value drops as the analysis is performed with more layers considered failed.

The results of the X-33 fuel tank analysis are very encouraging. The analysis represents the actual failure very well, which means the analysis should be accurate in predicting the onset and extent of microcracking for other sets of conditions for the laminated fuel tank. This analysis predicted microcracking through the entire thickness of the wall, just as it occurred in the real test. The study of the problem also shows that the layers did not all fail at once but progressed through the thickness of the laminate in stages. That is to say that the four layers that had microcracking at the original conditions caused just enough of an increase in the stress of the remaining uncracked lamina to cause further microcracking. This continued until the microcracking had worked its way through each ply. This is very probably the way the X-33 tank failed, because the failure did not happen suddenly.

DETERMINATION OF MICROCRACKING THRESHOLD

It has been established that the conditions endured by the X-33 will cause excessive microcracking. Now other conditions will be considered to find a threshold for the use of the BMI-carbon fiber laminate without failure. In this section the results will not be given in the level of detail provided in the previous section, only the results of the failure criterion will be given.

It was found that in the previous section that the thermal stress under the specified conditions was more than 90% of the strength of the material. This is the first

condition that will be explored in determining the threshold for microcracking. Figure 7 is a plot of the R value for the BMI-carbon fiber composite as a function of temperature.

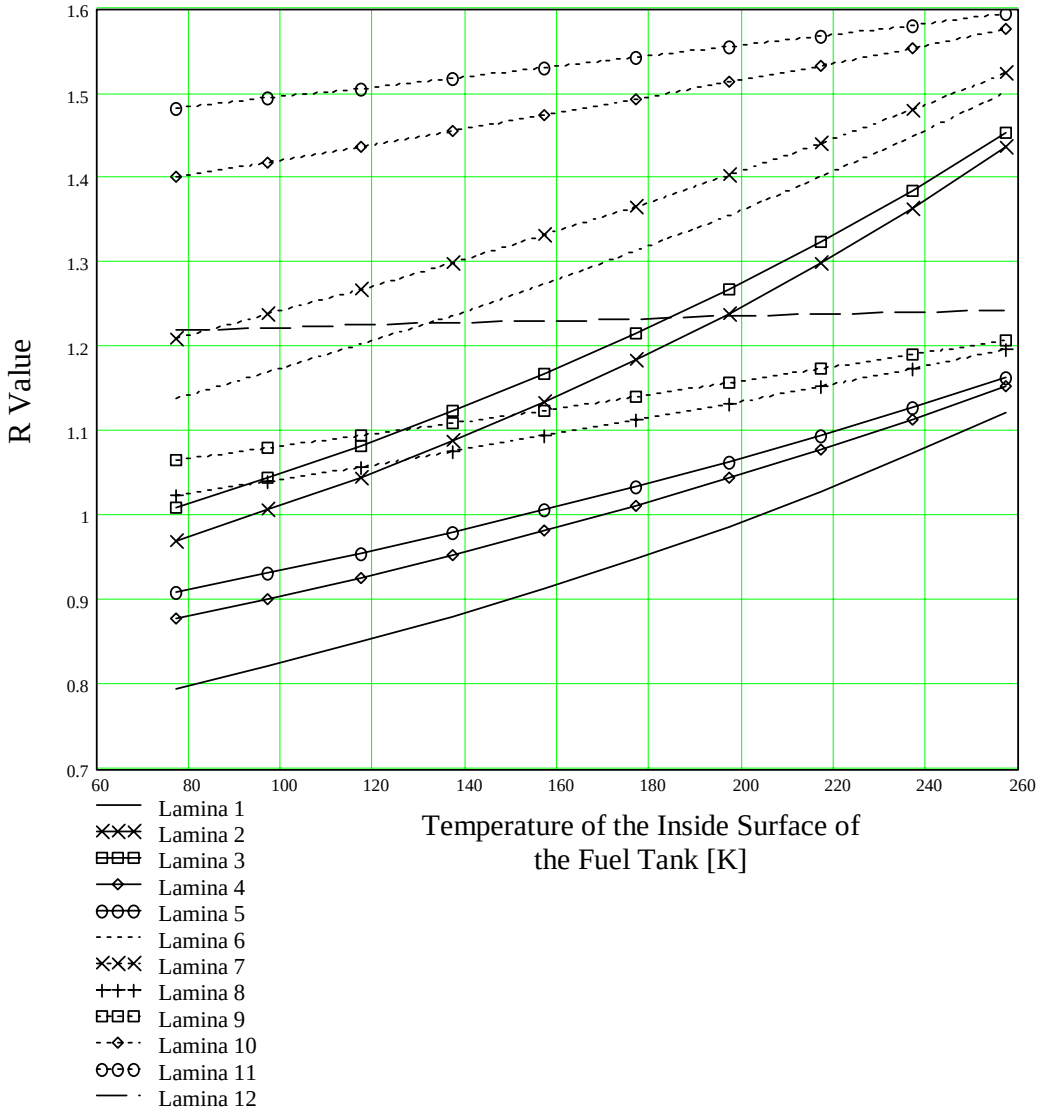

Figure 7. R value as a function of temperature, pressure is 290 kPa (42 psi).

In Figure 7 the R values are plotted for each ply of the laminate as the temperature of inside wall of the fuel tank is increased. The internal pressure is constant at 290 kPa (42 psi). Raising the temperature of the inside wall of the fuel tank could be accomplished through insulating the laminate with a liner. By raising the temperature at this point the thermal axial stress in the lamina is lowered due to the average temperature in the wall increasing. The thermal bending stress is also lowered because the temperature differential between the outside of the tank, which is constant at 300 K, and the inside of the tank is decreased as the inside wall temperature is increased. This plot provides a starting point to finding the lowest inside wall temperature that will not cause extensive microcracking.

Looking at the R = 1 line on the graph, the temperature at which each layer microcracks can be seen. At approximately 205 K, Figure 7 shows that none of the lamina have R values below one, therefore no microcracking occurs until the inside of the tank is below this temperature. It can also be seen that there is a large gap in the occurrences of the first and second lamina failures and the third and fourth failures. The first failure occurs at about 205 K and the second failure occurs at about 170 K. This may be important because when a progressive analysis is done the increase in stress due to the first failure may not be large enough to cause continued microcracking in additional lamina. There is a similar gap between the third and fourth failures.

The internal pressure of the fuel tank also contributed a significant amount to the total stress in the wall. The graph in Figure 7 is reproduced for the internal pressures of 241 kPa (35 psi) and 207 kPa (30 psi). These graphs are shown below as Figure 8 and

Figure 9. An additional plot is also given as Figure 10 which holds the temperature constant at 77 K (-196 ºC) and gives the R values as a function of internal pressure. Since the stress due to the fuel load was very small it will not be examined in finding the microcracking threshold.

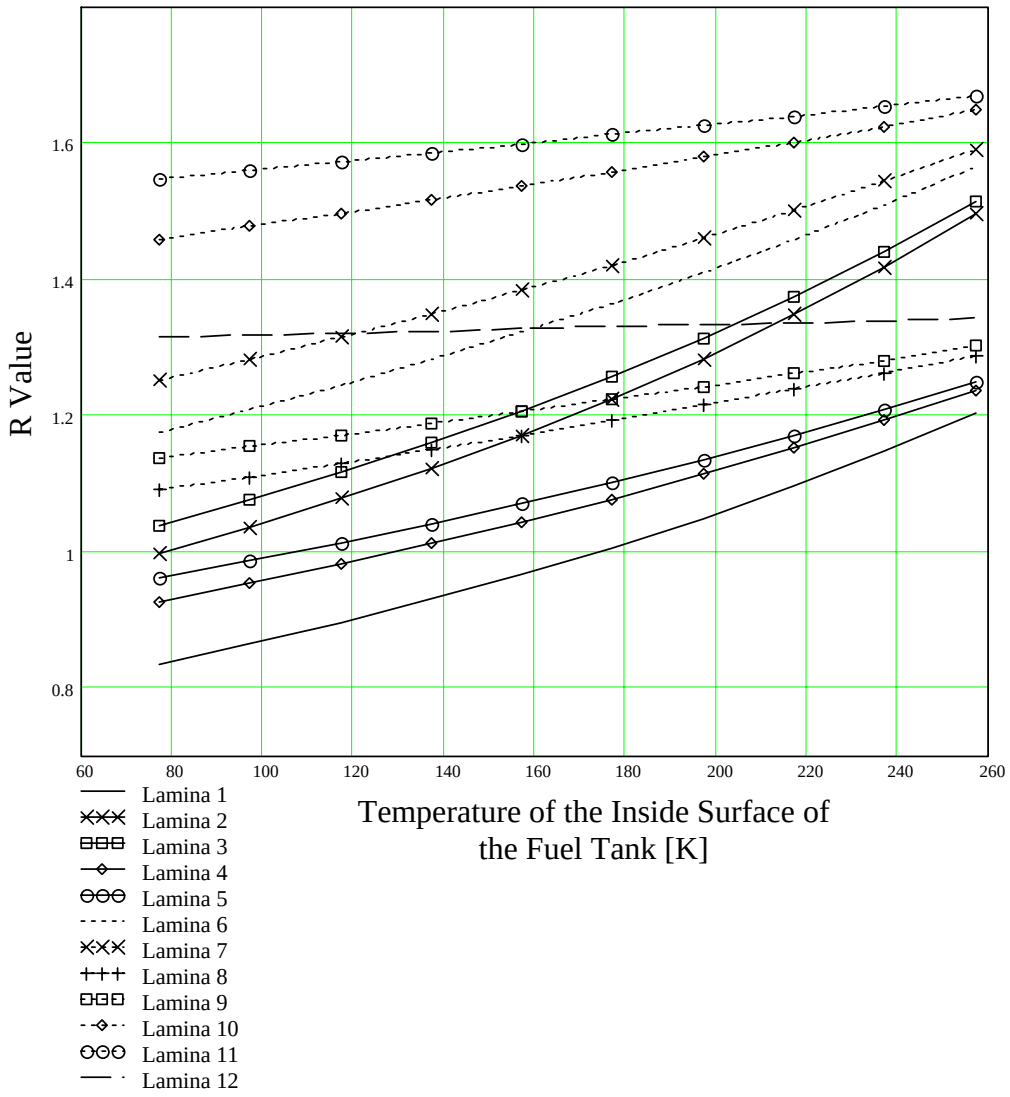

Figure 8. R value as a function of temperature, pressure is 241 kPa (35 psi).

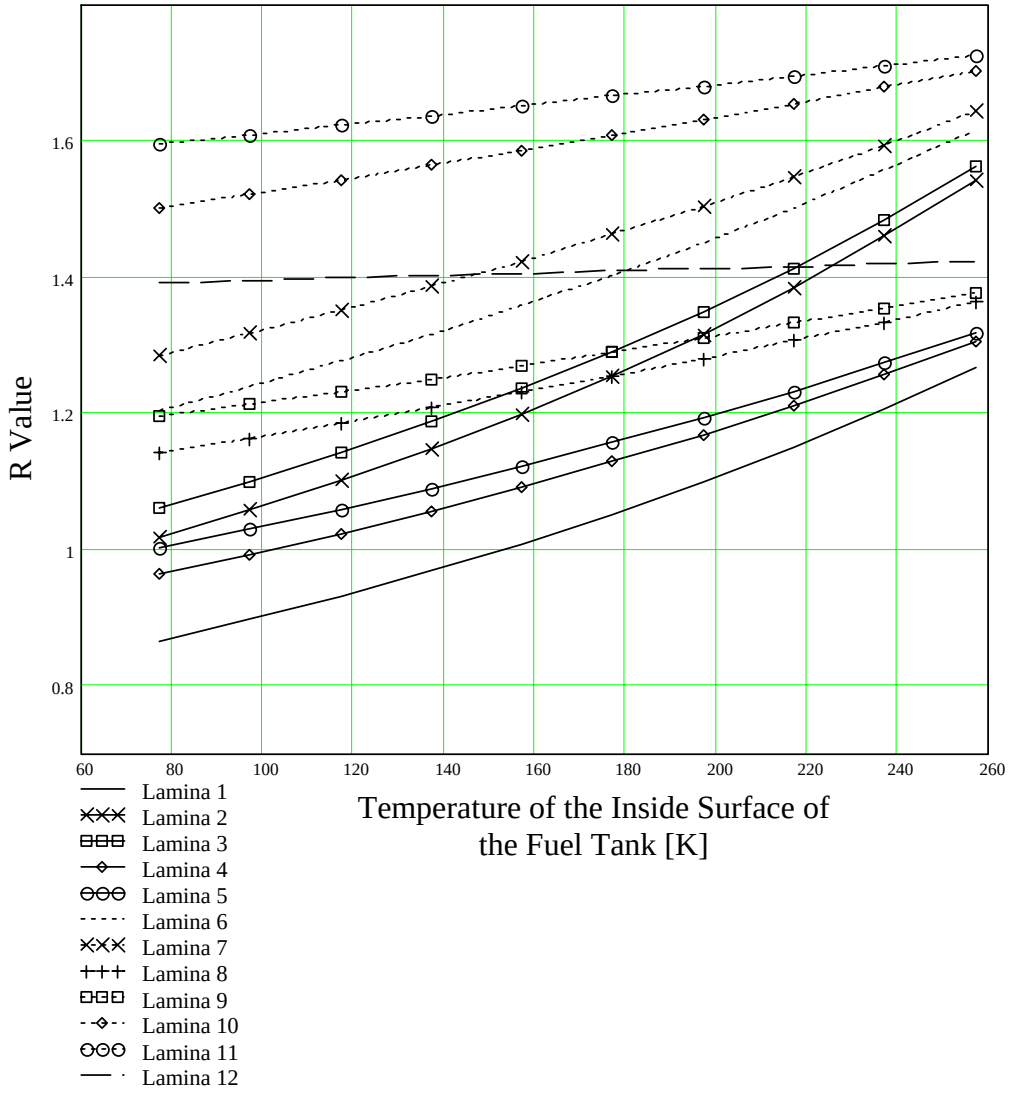

Figure 9. R value as a function of temperature, pressure is 207 kPa (30 psi).

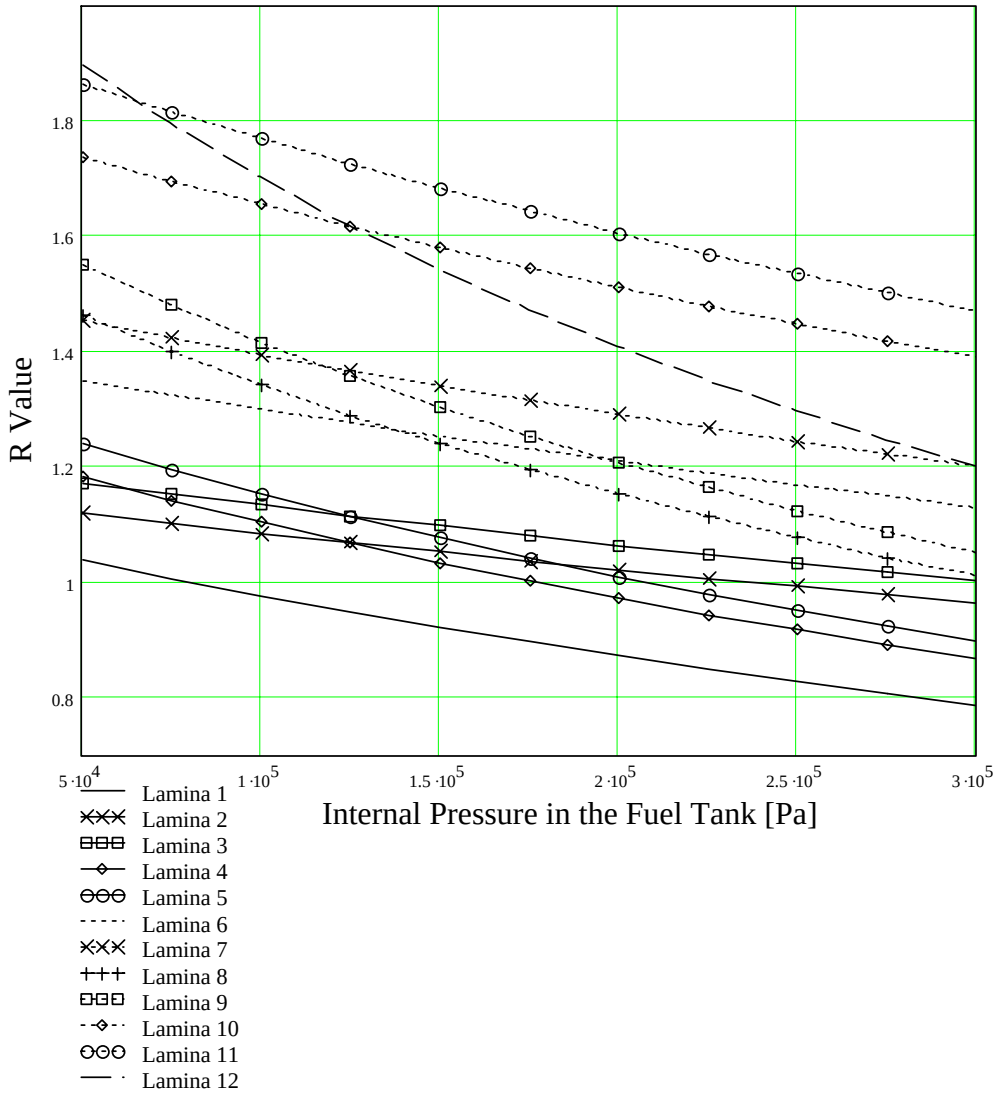

Figure 10. R value as a function of internal pressure, temperature is 77 K (-196 ºC).

As in Figure 7, key points for analysis can be obtained from Figure 8, Figure 9, and Figure 10. In Figure 8 and Figure 9 the temperature at which microcracking initiates for the given pressure can be found directly by observing where the first lamina R value

drops below one. Likewise, in Figure 10 the pressure at which the first microcracks initiate can be found. Other key points are located where the largest temperature difference or pressure difference exists between lamina failures. At these points there is a possibility that failure may not progress beyond that point.

A progressive failure analysis was performed on several key sets of conditions based on the above graphs. The following table, Table 9, gives the temperature and internal pressure of the condition set and a description of the failure analysis results.

Table 9. Progressive failure analysis of multiple condition sets.

Inside Wall Temperature K (ºC)		Internal Pressure kPa (psi)		Progressive Failure Results
77	(-196)	290	(42)	X-33 - Total Failure Progressed
205	(-68)	290	(42)	No Failures
195	(-78)	290	(42)	1 Layer Fails - No Progressive Failure
< 195	(-78)	290	(42)	Total Failure Progressed
175	(-98)	241	(35)	No Failures
150	(-123)	241	(35)	1 Layer Fails - No Progressive Failure
105	(-168)	241	(35)	3 Layers Fail - Progression Stopped
< 105	(-168)	241	(35)	Total Failure Progressed
155	(-118)	207	(30)	No Failures
120	(-153)	207	(30)	1 Layer Fails - No Progressive Failure
90	(-183)	207	(30)	3 Layers Fail - Progression Stopped
< 90	(-183)	207	(30)	Total Failure Progressed
77	(-196)	76	(11)	No Failures
77	(-196)	158	(23)	1 Layer Fails - No Progressive Failure
77	(-196)	193	(28)	3 Layers Failed - Progression Stopped
77	(-196)	> 193	(28)	Total Failure Progressed

Table 9 lists the results for the three constant pressure condition sets and one constant temperature condition set. For each set of conditions, combinations of inside wall temperature and internal pressure are given where no microcracking occurs in any layer of the laminate. When the progressive failure analysis shows that only one layer fails the conditions are considered to be the microcrack initiation conditions. These conditions sets are given. The next conditions that were given are when the failure progression through more than one lamina but stopped before the microcracking went through the entire laminate. Lastly, total failure conditions were listed. A graphical representation of the results is displayed in Figure 11.

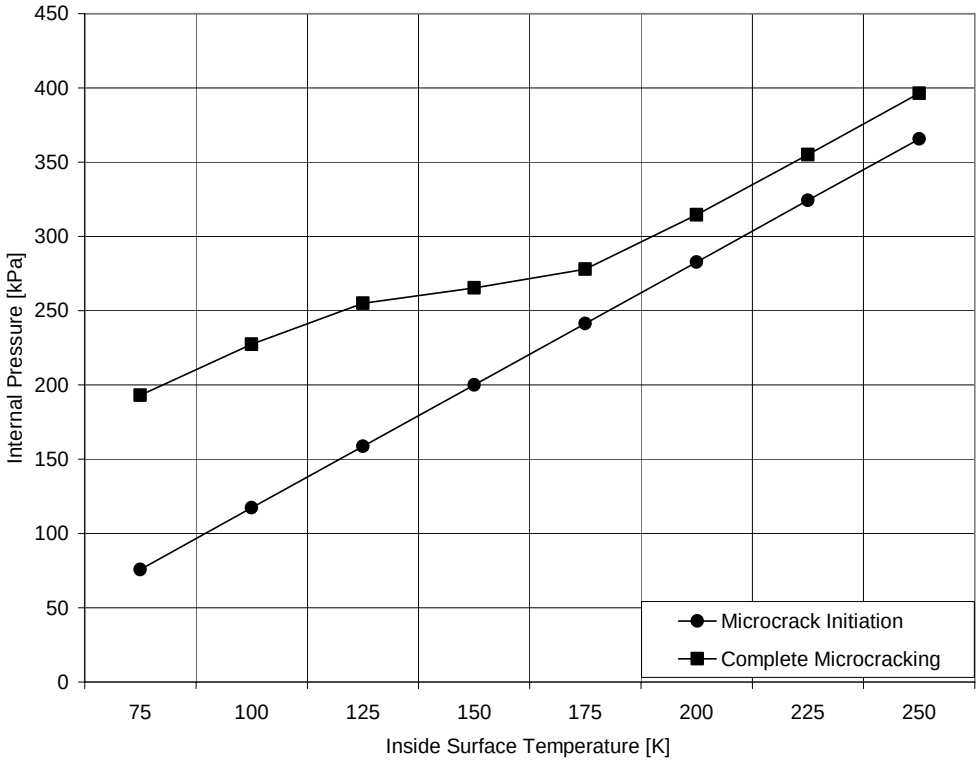

Figure 11. Conditions for microcrack initiation and complete microcracking.

The conditions for microcrack initiation and complete laminate microcracking are shown graphically in Figure 11. Any set of conditions below the line labeled microcrack initiation will not produce microcracking in any layer of the laminate. The area between the two lines represents the sets of conditions that will produce some microcracking, but the microcracking will not progress all the way through the thickness of the laminate. Above the complete microcracking line are the conditions that will cause microcracking through the entire thickness of the laminate.

One interesting observation is that the microcracking initiation line and the complete microcracking line are parallel in the high pressure and high temperature region of the graph, but the complete microcracking line becomes nonlinear at the lower pressure and lower temperature region. This is explained by the fact that in the high pressure and high temperature range of the graph the thermal stresses get very small and the pressure stress dominates. When the dominating stress is due to pressure the layers of the composite fail in two groups according to the way the lamina is aligned with the circumferential stress, which is twice the longitudinal stress. Therefore in this region of the graph the initiation of cracks is caused when the circumferential pressure stress exceeds the strength and the complete cracking occurs when the longitudinal stress exceeds the strength. The lines remain parallel as the pressure and temperature are decreased until the thermal bending stress starts getting relatively large. Since the thermal bending stress actually decreases the stress for the layers of the laminate on the outside of the fuel tank wall, it becomes harder for microcracking to progress completely through the laminate. This causes the complete microcracking line to separate from the

microcracking initiation line. The bending stress adds to the inside layers of the laminate so the microcracking initiation line does not become nonlinear as the temperature is decreased.

In this chapter it has been shown that the stress evaluation and analysis methods have accurately predicted the X-33 failure. This indicates that the calculations are a good mathematical representation of the underlying problem and can be used to determine the onset of transverse microcracking in the BMI-carbon fiber laminate when used in the fabrication of a cryogenic fuel tank. The conditions for the initiation of microcracks was determined and shown both graphically and in tabular form, along with conditions for total microcracking through the laminate. In the following chapter a summary of the conclusions that can be drawn from this study will be given. Recommendations for the design and use of the BMI-carbon fiber laminate in the cryogenic fuel tank will also be given, as well as recommendations for further work in this subject area.

CHAPTER V

SUMMARY AND CONCLUSIONS

A stress analysis has been performed and from the results given in the previous chapter the following conclusions and recommendations can be made. It was shown with support from the X-33 failure example that an appropriate stress analysis was developed and performed. The results revealed that at launch conditions the fuel tank would have extensive transverse microcracking. A summary of the transverse stresses induced when the tank is in launch conditions is given in Table 10. In this table, the stresses and the percentages of the total stress are given for each layer of the fuel tank wall.

Table 10. Summary of transverse stresses at launch condition.

	Transverse Stresses [MPa]						Total Stress
Layer	Thermal		Internal Pressure		Load		[MPa]
1	84.6	(71.3%)	34.1	(28.7%)	0.0	(0.0%)	118.7
2	80.1	(82.6%)	16.9	(17.2%)	0.0	(0.1%)	98.0
3	77.3	(82.0%)	16.9	(17.9%)	0.1	(0.1%)	94.3
4	73.6	(68.4%)	34.0	(31.6%)	0.0	(0.0%)	107.6
5	70.0	(67.3%)	34.0	(32.7%)	0.0	(0.0%)	103.9
6	66.7	(79.7%)	16.9	(20.2%)	0.1	(0.2%)	83.7
7	61.8	(78.4%)	16.9	(21.4%)	0.1	(0.2%)	78.8
8	58.5	(63.3%)	33.9	(36.7%)	0.0	(0.0%)	92.4
9	54.9	(61.8%)	33.9	(38.2%)	0.0	(0.0%)	88.7
10	51.2	(75.1%)	16.9	(24.8%)	0.1	(0.2%)	68.2
11	47.5	(73.6%)	16.9	(26.2%)	0.1	(0.2%)	64.5
12	43.8	(56.5%)	33.8	(43.5%)	0.0	(0.0%)	77.6

The thermal stress ranges from 56.5% to 84.6% of the total stress, and is the most significant source of stress in the laminate. The thermal stress is a function of the difference between the stress free temperature and the temperature to which the material is exposed. Therefore any way to decrease the difference between these temperatures will be the most efficient way to reduce stress. This could be accomplished through insulating the material or possibly modifying the material to reduce the stress free temperature.

Of the remaining stress sources only the internal pressure induced stress, which ranges from 17.2% to 43.5%, can be used to make a considerable decrease in total stress. Lowering the internal pressure would reduce the total stress. The internal pressure is determined, however, by requirements for fuel storage. The load stress makes such an insignificant addition to the total stress that it cannot be used to make any substantial reduction of stress.

Detailed in Figure 11 are the condition sets required to prevent microcracking. These conditions must be utilized in order to avoid a failure similar to that of the X-33 project. Changes must be made in the design of the fuel tank in order to use the BMI-carbon fiber laminate without extensive microcracking.

As mentioned an insulating layer could be used to decrease thermal stress or a pressure reduction would also diminish total stress, however, there are a few other considerations that could be made. The X-33 failure resulted from increased permeability caused by microcracking. If a liner could be used to prevent such an

increase in permeability, perhaps microcracking could be allowed without the risk of total failure.

Also lamination scheme optimization could be better explored for this application. In this laminate the largest lamina stress was applied to the transverse direction, the weaker direction, of a layer. It occurred in the inside layer, where the largest thermal bending stress was coupled with the circumferential pressure stress. This initiated microcracking sooner than if the transverse direction of the inside lamina was aligned with the longitudinal pressure stress.

As seen in the recommendations, there is room for further work in this area. Lamination scheme optimization and research into lining the laminate for both thermal protection and decreased permeability should be investigated. Through further work and modification of the design to meet the conditions set out in this thesis, a BMI-Carbon fiber laminate could be successfully used in a RLV cryogenic fuel tank.

REFERENCES

1. Goetz, R.C. and Ryan, R.S. (2000). Final Report of the X-33 Liquid Hydrogen Tank Test Investigation Team, Marshall Space Flight Center, Huntsville, AL.

2. Ju, J. and Morgan, R.J. (2003). Characterization of BMI-Carbon Fiber Composite Microcrack Development Under Thermal Cycling, *Annual Technical Conference – ANTEC*, Conference Proceedings, **2**: 2059-2063.

3. Ju, J., Li, Y., Lu, J., Moon, S., Ribeiro, R., Ronck, B., Tschen, F., and Morgan, R.J. (2003). Fundamental Materials Structure-Property Studies for Electron Beam Cured Composites, *International SAMPE Symposium and Exhibition Proceedings*, **48**: 1968-1980.

4. Hayes, B.S., Seferis, J.C., Tillman, M.S., and Timmerman, J.F. (2002). Matrix and Fiber Influences on the Cryogenic Microcracking of Carbon Fiber/Epoxy Composites, *Composites: Part A*, **33**: 323-329.

5. Hahn, H.T. and Kim, R.Y. (1979). Effect of Curing Stresses on the First Ply-failure in Composite Laminates, *Journal of Composite Materials*, **13**: 2-16.

6. Hahn, H.T. and Pagano, N.J. (1975). Curing Stresses in Composite Laminates, *Journal of Composite Materials*, **9**: 91-106.

7. Walker, S.P. (2004). Thermal Effects on the Compressive Behavior of IM7/PETI5 Laminates, *Journal of Composite Materials*, **38**: 149-162.

8. Hahn, H.T. (1976). Residual Stresses in Polymer Matrix Composite Laminates, *Journal of Composite Materials*, **10**: 266-278.

9. Pagano, N.J. and Hahn, H.T. (1977). Evaluation of Composite Curing Stresses. Composite Materials: Testing and Design (Fourth Conference), ASTM STP 617, American Society for Testing and Materials, pp. 317-329.

10. Reddy, J.N. (2004). *Mechanics of Laminated Composite Plates and Shells: Theory and Analysis*, 2nd Edition, CRC Press, Boca Raton, FL.

11. Craig, R.R. (2000). *Mechanics of Materials*, 2nd Edition, John Wiley & Sons, New York.

12. *ASME Boiler and Pressure Vessel Code*, Sec. 10, RD-1188.5, 2001, pp 61-62.

13. Swanson, S.R. and Trask, B.C. (1988). An Examination of Failure Strength in [0/±60] Laminates Under Biaxial Stress, *Composites*, **19**(5): 400-406.

14. Austin, R.E., Freeman, D.C., and Talay, T.A. (1997). Reusable Launch Vehicle Technology Program, *Acta Astronautica*, **41**: 777-790.

15. Miller, D.B., Morgan, R.J. (1979). The Structure, Modes of Deformation and Failure, and Mechanical Properties of Diaminodiphenyl Sulphone-cured Tetraglycidyl 4,4' Diaminodiphenyl Methane Epoxy, *Journal of Materials Science*, **14**: 109-124.

16. Bechel, V.T., Camping, J.D., Donaldson, S.L., Fredin, M.B., and Kim, R.Y. (2003). Effect of Stacking Sequence on Microcracking in Cryogenically Cycled Carbon/Bismaleimide Composite, *Composites: Part A*, **34(7)**: 663-672.

APPENDIX A

Documented in this appendix are the calculations to obtain the thermal stress in the first layer of the laminate at the X-33 failure conditions. First the material properties and reference temperatures are defined as follows:

$$E_x = 151 \cdot 10^9 \, \text{Pa}$$

$$E_y = 11 \cdot 10^9 \, \text{Pa}$$

$$\nu_{12} = 0.34$$

$$\nu_{21} = 0.025$$

$$\alpha_x = -0.43 \cdot 10^{-6} \frac{\text{m}}{\text{m} \cdot \text{K}}$$

$$\alpha_y = 18.10 \cdot 10^{-6} \frac{\text{m}}{\text{m} \cdot \text{K}}$$

$$t = 2.117 \, \text{mm}$$

$$T_0 = 322.5 \, \text{K}$$

$$T_1 = -8.78 \frac{\text{K}}{\text{mm}}$$

Using the above properties the stiffness matrix for the layer is found using equation (3.6), equation (3.7), and equation (3.8).

$$Q = \begin{bmatrix} \dfrac{E_x}{1 - \nu_{xy}\nu_{yx}} & \dfrac{\nu_{xy}E_y}{1 - \nu_{xy}\nu_{yx}} \\ \dfrac{\nu_{xy}E_y}{1 - \nu_{xy}\nu_{yx}} & \dfrac{E_y}{1 - \nu_{xy}\nu_{yx}} \end{bmatrix}$$

$$Q = \begin{bmatrix} 152.282 & 3.772 \\ 3.772 & 11.093 \end{bmatrix} \cdot 10^{9}\,\text{Pa}$$

The thermal expansion coefficient matrix is simply given as

$$\alpha = \begin{bmatrix} -0.43 \\ 18.1 \end{bmatrix} \cdot 10^{-6}\,\frac{\text{m}}{\text{m}\cdot\text{K}}$$

The above property matrices are combined with equation (3.4) and equation (3.5) to obtain the force and moment resultants respectively. After substitution, equation (3.4) becomes

$$\begin{Bmatrix} N_x^T \\ N_y^T \end{Bmatrix} = \int_{-12.7\,\text{mm}}^{-10.583\ \text{mm}} 322.5\text{K} \begin{bmatrix} 152.282 & 3.772 \\ 3.772 & 11.093 \end{bmatrix} \cdot 10^{9}\,\text{Pa} \begin{Bmatrix} -4.3\cdot 10^{-7} \\ 1.81\cdot 10^{-5} \end{Bmatrix} \frac{\text{m}}{\text{m}\cdot\text{K}}\,dz$$

Solving the integral gives the force resultant.

$$\begin{Bmatrix} N_x^T \\ N_y^T \end{Bmatrix} = \begin{Bmatrix} 1.9\cdot 10^{3} \\ 1.36\cdot 10^{5} \end{Bmatrix} \frac{\text{N}}{\text{m}}$$

Equation (3.5) becomes

$$\begin{Bmatrix} M_x^T \\ M_y^T \end{Bmatrix} = \int_{-12.7\,\text{mm}}^{-10.583\ \text{mm}} -8.73\,\frac{\text{K}}{\text{mm}} \begin{bmatrix} 152.282 & 3.772 \\ 3.772 & 11.093 \end{bmatrix} \cdot 10^{9}\,\text{Pa} \begin{Bmatrix} -4.3\cdot 10^{-7} \\ 1.81\cdot 10^{-5} \end{Bmatrix} \frac{\text{m}}{\text{m}\cdot\text{K}}\,z^2\,dz$$

This equation is solved and the bending resultant is found.

$$\begin{Bmatrix} M_x^T \\ M_y^T \end{Bmatrix} = \begin{Bmatrix} -7.01 \\ -500.3 \end{Bmatrix} \text{N}$$

Using the above results, the axial and bending stresses due to the thermal conditions can be determined. Equation (3.9) defines how the thermal axial stress is obtained from the normal force resultant.

$$\{\sigma^N\} = \begin{Bmatrix} \sigma_x^N \\ \sigma_y^N \end{Bmatrix} = \frac{1}{t} \begin{Bmatrix} N_x^T \\ N_y^T \end{Bmatrix}$$

Substituting the normal resultant and thickness yields

$$\begin{Bmatrix} \sigma_x^N \\ \sigma_y^N \end{Bmatrix} = \frac{1}{2.117\,\text{mm}} \begin{Bmatrix} 1.9 \cdot 10^3 \\ 1.36 \cdot 10^5 \end{Bmatrix} \frac{\text{N}}{\text{m}}$$

$$\begin{Bmatrix} \sigma_x^N \\ \sigma_y^N \end{Bmatrix} = \begin{Bmatrix} 0.89 \\ 64.2 \end{Bmatrix} \text{MPa}$$

The result gives the thermal axial stress for both the global x and y direction of the layer, or, in respect to single layer, the fiber and transverse direction respectively.

The thermal bending stresses are calculated using equation (3.10) and Equation (3.11).

$$\{\sigma^M\} = \begin{Bmatrix} \sigma_x^M \\ \sigma_y^M \end{Bmatrix} = \frac{1}{(t)(D)} \begin{Bmatrix} M_x^T \\ M_y^T \end{Bmatrix}$$

where

$$D = z + \frac{t}{2}$$

Plugging in the known quantities gives

$$\begin{Bmatrix} \sigma_x^M \\ \sigma_y^M \end{Bmatrix} = \frac{1}{(2.117\,\text{mm})(D)} \begin{Bmatrix} -7.011 \\ -500.3 \end{Bmatrix} \text{N}$$

where

$$D = -12.117\,\text{mm} + \frac{2.117\,\text{mm}}{2}$$

$$D = -11.64\,\text{mm}$$

Therefore,

$$\begin{Bmatrix} \sigma_x^M \\ \sigma_y^M \end{Bmatrix} = \begin{Bmatrix} 0.28 \\ 20.4 \end{Bmatrix} \text{MPa}$$

The thermal stresses for the first layer of the laminate have been calculated. The remaining layers are calculated in exactly the same manner. The stresses for all the layers are reported in Table 3.

APPENDIX B

A sample internal pressure stress calculation is given in this appendix. The conditions used are the X-33 failure conditions. Both the longitudinal and circumferential pressure stress in the first layer of the lamina is found in this example. The calculations are made using equation (3.13) and equation (3.14).

$$\sigma_x^P = \frac{P}{\left(\frac{R_O}{R_I}\right)^2 - 1}$$

$$\sigma_y^P = \frac{P\left(1 + \left(\frac{R_O}{r}\right)^2\right)}{\left(\left(\frac{R_O}{R_I}\right)^2 - 1\right)}$$

Where

$$P = 289.6\,\text{kPa}$$

$$R_0 = 3\,\text{m}$$

$$R_I = 2.9746\,\text{m}$$

$$r = 2.976\,\text{m}$$

The longitudinal stress due to internal pressure is, therefore,

$$\sigma_x^P = \frac{289.6\,\text{kPa}}{\left(\frac{3\,\text{m}}{2.975\,\text{m}}\right)^2 - 1} = 16.88\ \text{MPa}$$

and the circumferential stress is

$$\sigma_y^P = \frac{289.6\,\text{kPa}\left(1+\left(\frac{3\,\text{m}}{2.976\,\text{m}}\right)^2\right)}{\left(\left(\frac{3\,\text{m}}{2.9746\,\text{m}}\right)^2-1\right)} = 34.05\ \text{MPa}$$

APPENDIX C

The applied load stress example calculation is demonstrated in this appendix. Equation (3.17) is used to find the total stress due to loading in the x and y directions, and equation (3.22) and equation (3.23) are used to find the distribution of the total stress between the two differently oriented groups of layers. That is, the group oriented with the fiber direction parallel to the global x direction and the group oriented with the fiber direction at 90º to the global x direction.

The total stresses are given by

$$\begin{Bmatrix} \sigma_x^L \\ \sigma_y^L \end{Bmatrix} = \begin{Bmatrix} \dfrac{F_x}{A_x} \\ \dfrac{F_y}{A_y} \end{Bmatrix}$$

where forces, F_x and F_y, are

$$\begin{Bmatrix} F_x \\ F_y \end{Bmatrix} = m_f \begin{Bmatrix} a_x \\ a_y \end{Bmatrix}$$

$$m_f = 95{,}250\,\text{kg}$$

$$a_x = 1\,g$$

$$a_y = 0\,g$$

$$A_x = \pi\left[(3\text{m} + 0.0254\text{m})^2 - (3\text{m})^2\right] = 0.481\,\text{m}^2$$

$$A_y = (2 \cdot 10\text{m} + 4 \cdot 3\text{m}) \cdot 0.0254\text{m} = 0.813\,\text{m}^2$$

Therefore, the forces are written

$$\begin{Bmatrix} F_x \\ F_y \end{Bmatrix} = 95{,}250\,\text{kg} \begin{Bmatrix} 1\,\text{g} \\ 0 \end{Bmatrix}$$

$$\begin{Bmatrix} F_x \\ F_y \end{Bmatrix} = \begin{Bmatrix} 934{,}400 \\ 0 \end{Bmatrix} \text{N}$$

and the total applied load stress is

$$\begin{Bmatrix} \sigma_x^L \\ \sigma_y^L \end{Bmatrix} = \begin{Bmatrix} \dfrac{934{,}400\,\text{N}}{0.481\,\text{m}^2} \\ \dfrac{0}{0.813\,\text{m}^2} \end{Bmatrix}$$

$$\begin{Bmatrix} \sigma_x^L \\ \sigma_y^L \end{Bmatrix} = \begin{Bmatrix} 1.942 \\ 0 \end{Bmatrix} \text{MPa}$$

Now the total applied load stress, above, is distributed between the two groups of layers using equation (3.22) and equation (3.23). Since the first layer is oriented with the fiber direction parallel to the x axis, the equation are used with the 0 superscript.

$$\sigma_x^0 = \frac{E^0 \sigma_x^L}{(E^0 + E^{90})}$$

where

$$E^0 = E_x = 151\,\text{GPa}$$

$$E^{90} = E_y = 11\,\text{GPa}$$

$$\sigma_x^0 = \frac{151\,\text{GPa} \cdot 1.942\,\text{MPa}}{(151+11)\,\text{GPa}}$$

$$\sigma_x^0 = 1.81\,\text{MPa}$$

and

$$\sigma_y^0 = \frac{E^0 \sigma_y^L}{(E^0 + E^{90})}$$

therefore

$$\sigma_y^0 = \frac{11\,\text{GPa} \cdot 0\,\text{MPa}}{(151+11)\,\text{GPa}}$$

$$\sigma_y^0 = 0\,\text{MPa}$$

VITA

BRENT DURRELL PICKLE

PERMANENT ADDRESS:

PO Box 1167
Pottsboro, TX 75076

EDUCATIONAL BACKGROUND:

Master of Science, Mechanical Engineering. Texas A&M University, College Station, Texas. December 2004.

Bachelor of Science, Mechanical Engineering. University of Oklahoma, Norman, Oklahoma. May 2002.

CERTIFICATION:

Private Pilot Certificate. Andy Fay, CFI. College Station, TX. May 18, 2003.

WORK EXPERIENCE:

ConocoPhillips, Inc. Ponca City, OK 5/03-8/03
Intern – Mechanical Integrity & Reliability
Pipe stress and pressure vessel analysis

Conoco, Inc. Ponca City, OK 5/02-8/02
Intern – Reliability Group
Failure prediction of critical mechanical equipment

CFC Computer Technologies, Inc. Pottsboro, TX 5/97-12/98
Co-Owner – Vice President
Designed/built computer systems/networks, produced gross sales of $773,000.